https://doi.org/10.5194/egusphere-2023-321
Preprint. Discussion started: 23 March 2023

Coastal retreat rates of high-Arctic rock cliffs on Brøgger peninsula, Svalbard, accelerate during the past decade

Juditha Aga[1], Livia Piermattei[1,2], Luc Girod[1], Kristoffer Aalstad[1], Trond Eiken[1], Andreas Kääb[1], and Sebastian Westermann[1,3]

[1]Department of Geosciences, University of Oslo, Norway.
[2]Swiss Federal Institute for Forest, Snow and Landscape Research (WSL), Birmensdorf, Switzerland.
[3]Center for Biogeochemistry in the Anthropocene, University of Oslo, Norway.

Correspondence: Juditha Aga (juditha.aga@geo.uio.no)

Abstract. In many Arctic regions marine coastlines change rapidly in the currently warming climate. In contrast, coastal rock cliffs on Svalbard are considered to be comparably stable, based on previous studies that considered only a few years and limited coastal reaches. Long-term trends of coastal retreat rates in rock cliffs on Svalbard are unknown so far, but their quantification could improve the understanding of coastal dynamics on the Arctic archipelago. This study presents coastal retreat rates in rock cliffs along several kilometers of the Brøgger peninsula, Svalbard. The work is based on high-resolution orthoimages from 1970, 1990, 2010, and 2021, corroborated by high-precision dGNSS measurements along selected segments of the coastline and by rock surface temperature measurements during the period 2020-2021. Our analysis shows that coastal retreat rates accelerate statistically significant along the Brøgger peninsula in the time period of 2010 to 2021. This is true for both the northeast facing coastline, with retreat rates increasing from $0.04 \pm 0.06\,\mathrm{m\,a^{-1}}$ (1970-1990) and $0.04 \pm 0.04\,\mathrm{m\,a^{-1}}$ (1990-2010) to $0.07 \pm 0.08\,\mathrm{m\,a^{-1}}$ (2010-2021) and the southwest facing coastline, where retreat rates of $0.26 \pm 0.06\,\mathrm{m\,a^{-1}}$ (1970-1990), $0.24 \pm 0.04\,\mathrm{m\,a^{-1}}$ (1990-2010) and $0.30 \pm 0.08\,\mathrm{m\,a^{-1}}$ (2010-2021) are measured. Furthermore, the parts of the coastline affected by erosion increase along the northeast facing coastline from $47\,\%$ (1970-1990) to $65\,\%$ (2010-2021), while they stay consistently above $90\,\%$ along the southwest facing coastline. Measurements of rock surface temperature show mean annual values close to the thaw threshold with $-0.49\,°\mathrm{C}$ at the southwest facing coastline, while records at the northeast facing coastline are lower with $-1.64\,°\mathrm{C}$. The recently accelerated retreat rates coincide with increasing storminess and retreating sea ice, together with increasing ground temperatures, all factors that can enhance coastal erosion.

1 Introduction

Arctic permafrost environments can respond rapidly to changing climatic conditions (Biskaborn et al., 2019). This is especially true for Arctic coastlines where sea level rise, sea ice retreat, and loss of permafrost and glaciers have pronounced effects on coastal dynamics (Irrgang et al., 2022). Therefore, Arctic coasts are often eroding more rapidly than coasts in temperate regions, recently with an average retreat rate of $0.5\,\mathrm{m\,a^{-1}}$ (Lantuit et al., 2013). Higher rates are found in ice-rich permafrost bluffs and barrier islands, (e.g., along the Beaufort coast, Jones et al., 2018). Following the changing climatic conditions, erosion rates along the Arctic coastline have increased since the early 2000s (Irrgang et al., 2022), enhancing organic carbon

https://doi.org/10.5194/egusphere-2023-321
Preprint. Discussion started: 23 March 2023

and sediment fluxes into the nearshore zone (Fritz et al., 2017; Tanski et al., 2017) and threatening infrastructure, settlements and archaeological sites (Radosavljevic et al., 2016).

In contrast, lithified coastlines in the Arctic are assumed to be comparatively stable. On Svalbard, the retreat of coastal rock cliffs was estimated to be in the order of mm to cm per year: a yearly retreat of coastal cliffs by 2.7 to 3.1 mm from 2002 to 2004 was observed in Kongsfjorden (Wangensteen et al., 2007) and by up to 1.9 cm between 2014 to 2015 in Hornsund (Lim et al., 2020). In contrast, mixed-type coasts on Svalbard, i.e. bedrock cliffs covered by unconsolidated sediment, have been documented to show larger erosion rates of up to 80 cm per year (Guégan and Christiansen, 2017).

Warming is especially intense on Svalbard, as the archipelago is influenced by the northern part of the warm North Atlantic current, making it more susceptible to atmospheric and oceanic changes (Walczowski and Piechura, 2011). Air temperatures have increased in the past decades (Nordli et al., 2020) and are projected to rise also in the future, with the highest rates in the winter season (Hanssen-Bauer et al., 2019; Isaksen et al., 2016). Following this atmospheric trend, borehole data from the last decades show increasing permafrost temperatures on Svalbard (Boike et al., 2018; Christiansen et al., 2010; Etzelmüller et al., 2020; Isaksen et al., 2007). The effect of increasing air temperature on permafrost degradation and thaw is expected to be especially pronounced along the coastline, as the ground can be warmed both from the top and laterally from the bluff face (Irrgang et al., 2022).

In addition to increasing air and ground temperatures, sea ice coverage has been markedly reduced around Svalbard. A prime example is Kongsfjorden, which was typically covered by sea ice during the winter season (Gerland and Hall, 2006). However, since 2002, the sea ice duration has shortened and after 2006, the maximum extent of sea ice was drastically reduced (Johansson et al., 2020). Longer ice-free seasons enhance the influence of wave action and storms (Overeem et al., 2011). Furthermore, radiative warming by the relatively warm sea water can lead to higher ground surface temperatures along the coast (Schmidt et al., 2021). Both the exposure to waves and storms, and the warming trend in permafrost could contribute to increased vulnerability of the coasts in Svalbard.

Previous studies on coastal erosion in Svalbard cover only a few years (Guégan and Christiansen, 2017; Lim et al., 2020; Prick, 2004; Wangensteen et al., 2007) and long-term analyses are lacking so far. These can be especially valuable, as short-term studies may be biased by the presence or absence of single storm events that can contribute considerably to coastal erosion. The present study focuses on the erosion rate of the sediment-covered coastal cliffs along the Brøgger peninsula, Svalbard, based on high-resolution historical and digital aerial images (1970 to 2021). The main objectives of this study are (i) to detect long-term trends in coastal retreat along the Brøgger peninsula by performing separate analyses for the northeast and southwest facing coastline, (ii) to analyze rock surface temperatures for both expositions of the coastline, and (iii) to link these changes to available climate data.

2 Study area

The study area is the northwestern part of the Brøgger peninsula, located on the west coast of Spitsbergen, with a total coastline of about 14 km. We focus on approximately 5.5 km of coastline, where rock cliffs behind beach sediments show active coastal

https://doi.org/10.5194/egusphere-2023-321
Preprint. Discussion started: 23 March 2023

erosion of the bedrock (Etzelmüller et al., 2003). The bedrock is dominated by conglomerates, sandstones, shales and carbonates from the Carboniferous to Permian age, which often form overhanging coastal cliffs (Fig. 1). They are typically covered with several meters of unconsolidated marine deposits from the Holocene. As the unconsolidated sediments are more prone to erosion, they often form a slightly retreated line above the bedrock (Fig. 1).

Meteorological data such air temperature and solar radiation are measured by a weather station located in Ny-Ålesund (Fig. 1), which is approximately 8 km southeast of the study area and located at the northeast facing coastline of the Brøgger peninsula. The variables have been measured since 1992 and document an increase in mean annual air temperature of 1.3 ± 0.7 °C per decade with the strongest increase in winter season with 3.1 ± 2.6 °C per decade. Winter warming is associated with an increase in incoming longwave radiation of 15.6 ± 11.6 W m^{-2} per decade. As the duration of snow cover is shortened and, hence, the reflection of shortwave radiation is reduced, the net shortwave radiation is slightly increased in the spring and summer seasons (Maturilli et al., 2015).

The mean annual precipitation between 2010 and 2021 in Ny-Ålesund was 526 mm with an increasing trend in the last decades (Norwegian Meteorological Institute, 2022). Both snowfall and rainfall can occur at any time during the course of the year. However, the snow season typically lasts from October to June (Hop and Wiencke, 2019).

3 Data and methods

We used orthoimages derived from aerial nadir images acquired in 1970, 1990, 2010, and 2021 (Section 3.1) to analyze the retreat rate of the coastline (Section 3.3). In August 2021, almost at the same time as the airborne image acquisition, we conducted a dGNSS survey along selected parts of the coastline (Section 3.2) to collect validation data. Rock surface temperatures were measured from September 2020 to August 2021 (Section 3.4). Furthermore, we used topographically downscaled ERA5 reanalysis data (see appendix) to contextualize our results in light of ongoing climate change.

3.1 Orthoimages

The historical aerial images acquired in 1970 and 1990 were provided by the Norwegian Polar Institute (NPI). The 1970 data is composed of nine images (Table 1), which were taken with a RC8 camera (152 mm focal length) on an altitude of circa 2700 m in two flight lines. No calibration file was available to us and we used therefore the nominal calibration for this camera model. The grey-scale 1970 images were scanned from prints using an HP Expression XL10000 (A3 flatbed scanner), at 2400 dpi using 16 bit grey scale. The 31 images from 1990 (Table 1) were acquired with a RC20 camera (152 mm focal length) on an altitude of approximately 2700 m in seven flight lines. The calibration report was made available by NPI. The false-colour infrared images of 1990 were scanned by the Norwegian Polar Institute with a photogrammetric scanner at a resolution of 1800 dpi using 8 bit colour scale. The 1970 and 1990 aerial images were processed separately with MicMac, an open-source software for photogrammetry (Rupnik et al., 2017), with scripts available in Girod and Filhol (2022). The workflow identifies tie points to match the images and solves relative orientation, uses ground control points (GCPs) for bundle adjustment and refinement of the camera calibration, and finally generates a DEM and an orthoimage. We used the same GCPs for both the

https://doi.org/10.5194/egusphere-2023-321
Preprint. Discussion started: 23 March 2023

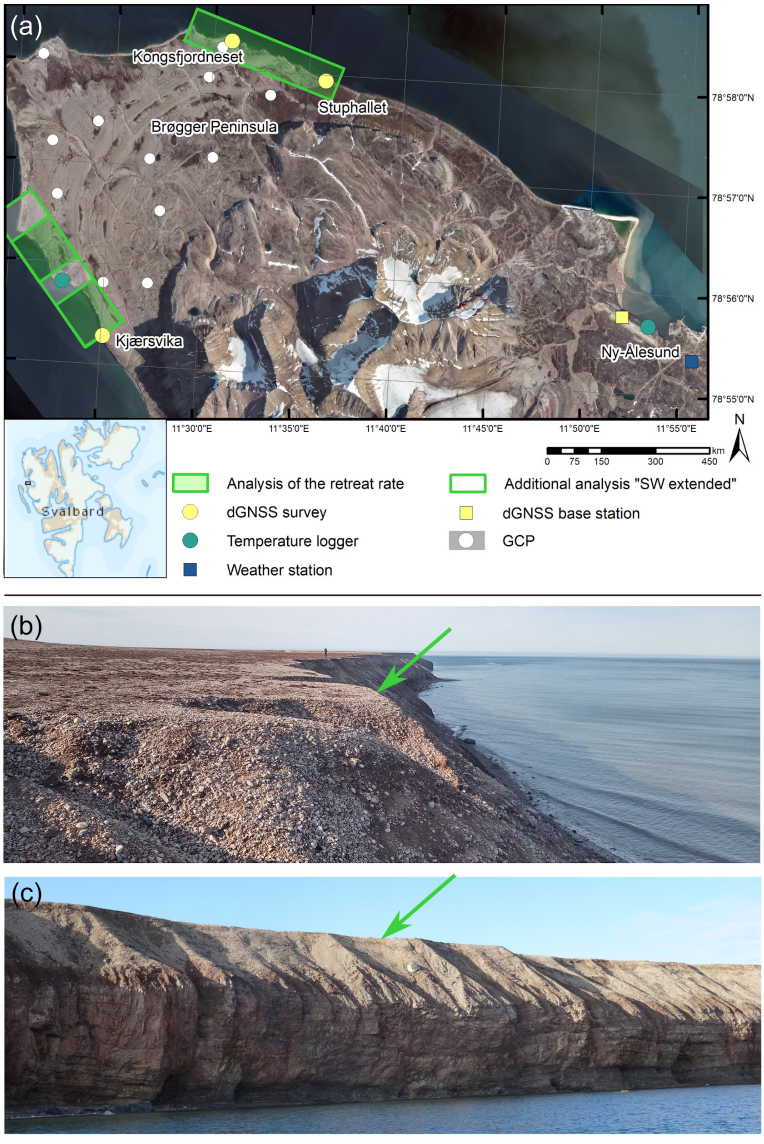

Figure 1. (a) Orthoimage of the study area, including the measurement sites. The coastal retreat rate is analyzed along the northeast and southwest facing coastline with an extended part in the southwest. The locations of the dGNSS surveys and the corresponding base station, the temperature loggers, the weather station and the ground control points (GCP) are shown as dots. Source: NP_Basiskart_Svalbard_WMTS_32633 © Norwegian Polar Institute. The (b) top and the (c) bluff face along the coastline of Brøgger peninsula show the rock cliffs covered with unconsolidated sediments. The green arrows and lines indicate the top of the cliff that is digitized.

1970 and 1990 images, which were identified and extracted from the 2010 DEM and orthoimage (Fig. 1). DEMs were produced for both 1970 and 1990. We estimated the a-priori accuracy of the GCPs to be around 0.5 m, which was also confirmed by the results of the bundle adjustments. Both the 1970 and 1990 airphotos are taken by a high-precision photogrammetric-class

https://doi.org/10.5194/egusphere-2023-321
Preprint. Discussion started: 23 March 2023

camera using several overlapping flight lines. The DEMs generated from them showed no significant artefacts in comparison to the 2010 DEM. We thus decided to use the respective DEMs for the 1970 and 1990 orthoprojections.

The 2010 orthoimage and DEM were readily downloaded at a resolution of 0.20 m from the Norwegian Polar Institute base data of Svalbard (https://geodata.npolar.no/ and Norwegian Polar Institute (2014b)). The 2021 aerial images were collected by Svalbard Integrated Arctic Earth Observing System (SIOS) with a ground sampling distance of 0.08 m. High-precision onboard dGNSS and navigation data were available for these newer images, so that the geolocation tags in the metadata files of the images could be used to georeference the images, allowing for an overall simpler workflow. The correct georeferencing was confirmed by comparison with the 1970, 1990 and 2010 images. The orthoimages were again processed in MicMac (Girod and Filhol, 2022), but this time by mosaicking individually orthorectified images. The resolution of the final product was set to 0.20 m to perform the analysis consist with the resolution of the other images and to reduce the file size. The attributes of the orthoimages are reported in Table 1.

Table 1. Orthoimages used in this study and the respective metadata, the number and accuracy of the ground control points (GCP).

Acquisition date	Image provider	No. of images	Orthoimage resolution [m]	No. of GCPs	Accuracy [m] of GCPs
28 Aug 2021	SIOS	306	0.20	0	N/A
1 Aug 2010	NPI	N/A	0.20	N/A	N/A
14-22 Aug 1990	NPI	31	0.25	13	0.5
22 Aug 1970	NPI	9	0.20	13	0.5

3.2 dGNSS survey

The dGNSS measurements were used to validate if the manual digitization of the coastline from 2021 (section 3.3) shows a systematic seaward or landward bias. They were well suited for that purpose as the dGNSS survey was conducted on August 31, 2021, while the aerial images were acquired on August 28, 2021. As no real-time connection to the base station in Ny-Ålesund could be established, logging of raw data in the field was necessary. Hereby, the receiver was placed in positions exactly at the cliff edge. dGNSS observations were made with an Altus APS3G GPS+Glonass receiver in a kinematic stop&go survey. The receiver was kept static at each point for 60 seconds with a 1-second log interval for raw data. Post-processing was made with the software RTK-lib ver. 3.4 (Takasu and Yasuda, 2009) relative to the permanent station NYA1 in Ny-Ålesund at a distance of 6 to 10 km.

The dGNSS surveys were conducted along three transects of the coastline of Brøgger peninsula: Kjærsvika, Kongsfjordneset, and Stuphallet (Fig. 1). The length of each transect is circa 40 m (10 points) at Kjærsvika, 275 m at Kongsfjordneset (45 points) and 182 m at Stuphallet (37 points). The number of points and the distance between them was adapted to the irregularity of the coastline, but on average we measured with intervals of 5-6 m. Standard deviations of dGNSS measured positions were a few cm and were considered error-free in the comparison with the digitized coastline, as the pixel size of the orthoimages are larger than the calculated errors.

https://doi.org/10.5194/egusphere-2023-321
Preprint. Discussion started: 23 March 2023

3.3 Calculation of the coastal retreat rates

The coastline was digitized along the top of the cliff (Fig. 1), which is slightly retreated compared to the actual shoreline, i.e. the boundary between water and land, due to unconsolidated sediments on top of the bedrock (see section 2). Nevertheless, we are confident that the shift of the top of the cliff is representative of the coastal retreat, as a consistent shift in both top of the bedrock and top of the cliff could be detected where the quality of the orthoimages allows it. As the top of the cliff could typically be recognized more easily, it was used for further analysis.

The coastline was digitized manually in a GIS environment using the WGS 1984 UTM Zone 33N at a scale of 1:400 by the same operator. We analyzed the northeast and southwest facing coast of the Brøgger peninsula (Fig. 1) as the remaining coastline between Kongsfjordneset and Kvadehuksletta is mainly characterized by beaches, which are outside the scope of this study. Furthermore, the digitization along the bedrock coast was interrupted sporadically due to (1) rivers feeding into the fjord and cutting into the bedrock, (2) closely spaced thermo-erosional gullies, which prevent a clear detection of the coastline, and (3) the quality of the orthoimages. The last point affects only the digitization of the southwest facing coastline in the 1970 data, resulting from unfavourable illumination conditions.

The coastal retreat rate was calculated by comparing the coastline position between the years 1970-1990, 1990-2010, and 2010-2021. Each coastline position is subject to an uncertainty U, calculated following Irrgang et al. (2018) and Radosavljevic et al. (2016):

$$U = \sqrt{\mathrm{E_{GR}}^2 + \mathrm{RMS}^2 + \mathrm{LOA}^2} \tag{1}$$

with $\mathrm{E_{GR}}$ being the ground resolution of the orthoimage, RMS representing the root mean square error created by the georeferencing of the aerial image, and LOA being the loss of accuracy due to digitizing errors. The RMS was estimated from manually measured offsets between the different orthoimages over stable terrain distributed over Kvadehuksletta (Fig. 1). The LOA was determined by repeating the digitization four times along the coastline segments where the dGNSS survey was conducted. Every meter along the three additional digitized lines, the distance to the original digitized coastline was calculated and the associated root mean square error served as the LOA for further uncertainty calculations.

The coastal retreat rates were computed with the Digital Shoreline Analysis System (DSAS) version 5.1, an extension to Esri ArcGIS (Himmelstoss et al., 2021), which has been successfully applied in previous studies to detect changes in Arctic coastlines (e.g. Günther et al., 2013; Irrgang et al., 2018; Jones et al., 2018; Radosavljevic et al., 2016). Hereby, transects crossing all digitized coastlines are automatically generated with a user-defined spacing and the distance between these intersections are calculated. Due to the large number of transects along the coastline, statistical analyses of the coastal retreat rates can be performed. We analyzed the time periods 1970-1990, 1990-2010, and 2010-2021, constrained by the availability of orthoimages. As a first step, the distance between the digitized coastlines was calculated separately for transects with a spacing of 5 m along the coastline (same spacing as in Radosavljevic et al. (2016)). Locally, irregularities of the coastlines may be distinct, e.g. protruding edges, and may lead to the case that a transect crosses the digitized coastline twice. Here, we always selected the smallest distance between two coastlines so as not to overestimate the coastal retreat rates (Fig. 2). We calculated the retreat

https://doi.org/10.5194/egusphere-2023-321
Preprint. Discussion started: 23 March 2023

rate RR for every transect by dividing the distance of the intersection Δx (Fig. 2) by the analyzed time period Δt

$$RR = \frac{\Delta x}{\Delta t}, \tag{2}$$

followed by the mean retreat rates as well as the percentage of transects that display a retreat.

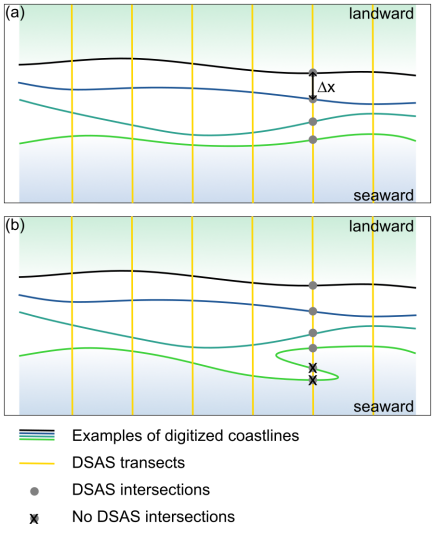

Figure 2. (a) Illustration of the analysis with DSAS, showing the digitized coastlines and the transects with intersections. The distance between two intersection is the retreat along one transect. (b) In case of several intersection with one coastline, the smallest distance was used for analysis.

In total, 2.67 km of the northeast facing coastline and 1.73 km of the southwest facing coastline were analyzed for all orthoimages, in addition to 1.15 km only for the time periods 1990-2010 and 2010-2021 along the southwest facing coastline, where the coastline in the orthoimage of 1970 could not be detected reliably. The uncertainty of the retreat rate, here dilution of accuracy (DOA), was calculated from the uncertainty of the coastline position U and the analyzed time span Δt (Irrgang et al., 2018; Radosavljevic et al., 2016):

$$\mathrm{DOA} = \frac{\sqrt{U_1^2 + U_2^2}}{\Delta t}. \tag{3}$$

To determine whether the increase (decrease) in the retreat rate is a statistically significant acceleration (deceleration) of the erosion, we performed a right-tailed (left-tailed) paired Student's t-test (Student, 1908) by comparing two consecutive retreat rates (e.g., 1970-1990 vs. 1990-2010) and evaluating the p-value using a threshold for significance of $\alpha = 0.005$ (Benjamin et al., 2018). p-values lower than this threshold can be considered statistically significant, which entails that the chance of observing a change in retreat as extreme as the one observed is extremely unlikely given the null hypothesis of no change (Ambaum, 2010; Benjamin et al., 2018).

https://doi.org/10.5194/egusphere-2023-321
Preprint. Discussion started: 23 March 2023

3.4 Rock surface temperature monitoring

For analyzing the thermal regime of the rock walls, an iButton (© Maxim) temperature logger was installed in a rock wall close to Kjærsvika, representing rock surface temperatures of the southwest facing coastline (RW-SW). No records could be gained in the field area at the northeast facing coastline. Therefore, previously published rock surface temperature data were used in this study (RW04), which were taken at an 8 km distance from the study area and follow the same installation technique, as described below (Schmidt et al., 2021). The naming of the temperature logger was adopted from the aforementioned study to simplify the comparison. Including temperature data from these two settings allows the analysis of the thermal regime on both expositions of the Brøgger peninsula (Fig. 1).

The measurements cover the time period from September 2020 to August 2021 with a sampling period of 4 hours. The iButtons were placed in cracks in the coastal cliffs, ensuring direct thermal contact between the sensor with the rock surface while protecting it from direct sunlight. The manufacturer states the measurement accuracy to 0.5 °C. The numerical precision of the sensor readout was set to 0.0625 °C. We used no additional calibration. The uncertainty of the sensor and/or logger system could be analyzed for the iButtons close to Ny-Ålesund, as several iButtons were placed in the same rock wall. Schmidt et al. (2021) found uncertainties of less than 0.1 °C for annual averages and less than 0.2 °C for seasonal values. However, this analysis was not possible for the iButton close to Kjærsvika as only a single sensor was operational during the study period. The annual average for RW04 was calculated without a seven-day period in August 2021, for which no data are available.

4 Results

4.1 Digitization of coastlines

Coastal retreat rates were analyzed for three different time periods 1970-1990, 1990-2010, and 2010-2021, based on the digitized coastlines on the respective orthoimages. Figure 3 shows a selected segment of the southwest facing coastline for all time periods, together with the digitized coastlines and the results of the dGNSS survey. The uncertainty of the digitized coastline is approximately 0.6 m for 1990, 2010, and 2021, while it is 1.07 m for the year 1970, based on multiple digitization of the coastline in selected transects (section 3.3). However, as the analyzed time periods are one decade or more, the uncertainty for the retreat rates per year is reduced to 0.08 m or less (Table 2).

In addition, the digitized coastline of 2021 was validated with the dGNSS measurements. The mean distance between the dGNSS points and the digitized coastline was 0.33 m, which is approximately 1-2 pixels on the orthoimage (Table 1). The calculated bias is 0.12 m, indicating a slight landward shift of the digitized coastline. However, this is mainly attributable to four dGNSS points with a distance of more than 2 m, where protruding edges weren't detected in the orthoimage due to an unfavourable illumination. Removing those led to a mean distance between the dGNSS points and the digitized coastline of 0.23 m and a bias of 0.00 m. Consequently, typically no systematic seaward or landward bias could be detected, however, some protruding edges might not be captured with the digitized coastline.

https://doi.org/10.5194/egusphere-2023-321
Preprint. Discussion started: 23 March 2023

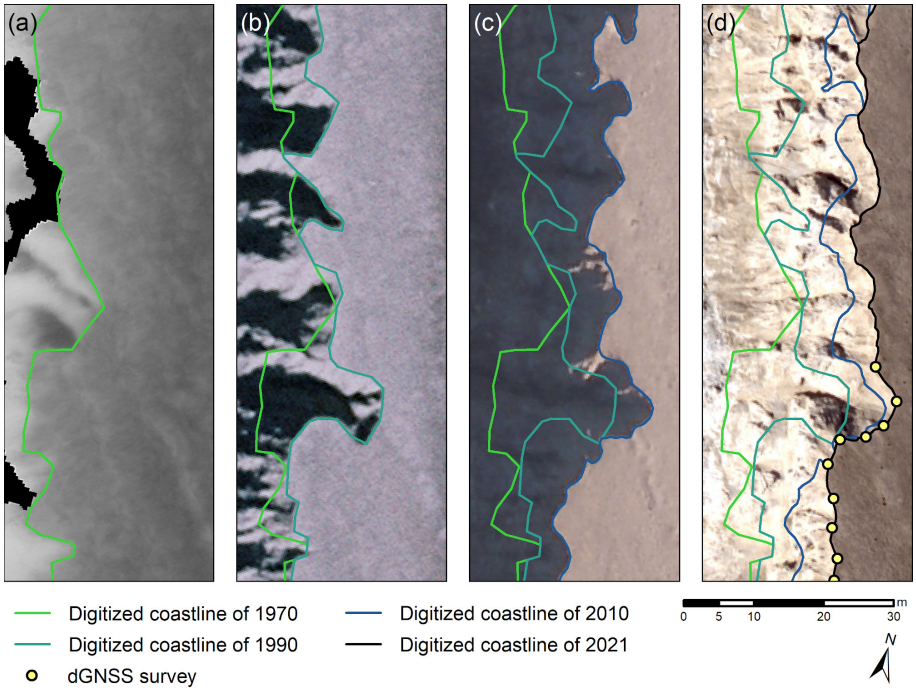

Figure 3. Orthoimages and digitized coastlines from (a) 1970, (b) 1990, (c) 2010, and (d) 2021 along a selected transect of the southwest facing coastline. The sea is to the left (west) of the image sections shown. The results of the dGNSS survey agree well with the digitized coastline of 2021. Source of the orthoimages: (a) and (b): Norwegian Polar Institute, not publicly available; (c): Norwegian Polar Institute, https://geodata.npolar.no/; (d): Svalbard Integrated Arctic Earth Observing Systems SIOS, not publicly available.

Table 2. Uncertainty associated with the digitization of the coastline. E_{GR} stands for the resolution of the orthoimage, RMS for the root mean square error associated with the georeferencing of the images and the noise from the processing, LOA for the loss of accuracy due to digitization, U for the uncertainty of the coastline position and DOA for the dilution of accuracy.

Year of orthoimage	E_{GR} [m]	RMS [m]	LOA [m]	U [m]	DOA [m]
2021	0.20	0.5	0.23	0.59	0.08
2010	0.20	0.5	0.28	0.61	0.04
1990	0.25	0.5	0.25	0.61	0.06
1970	0.20	1	0.33	1.07	

4.2 Coastal retreat rates on the Brøgger peninsula

The analysis for the different time periods was performed separately for the northeast and southwest facing coastline, due to markedly different retreat rates. The resulting retreat rates are visualized in Fig. 4 and all results (retreat rates and their

https://doi.org/10.5194/egusphere-2023-321
Preprint. Discussion started: 23 March 2023

uncertainties, percentage of transects calculating erosion and p-values for significant acceleration of the retreat rates) are summarized in Table 3.

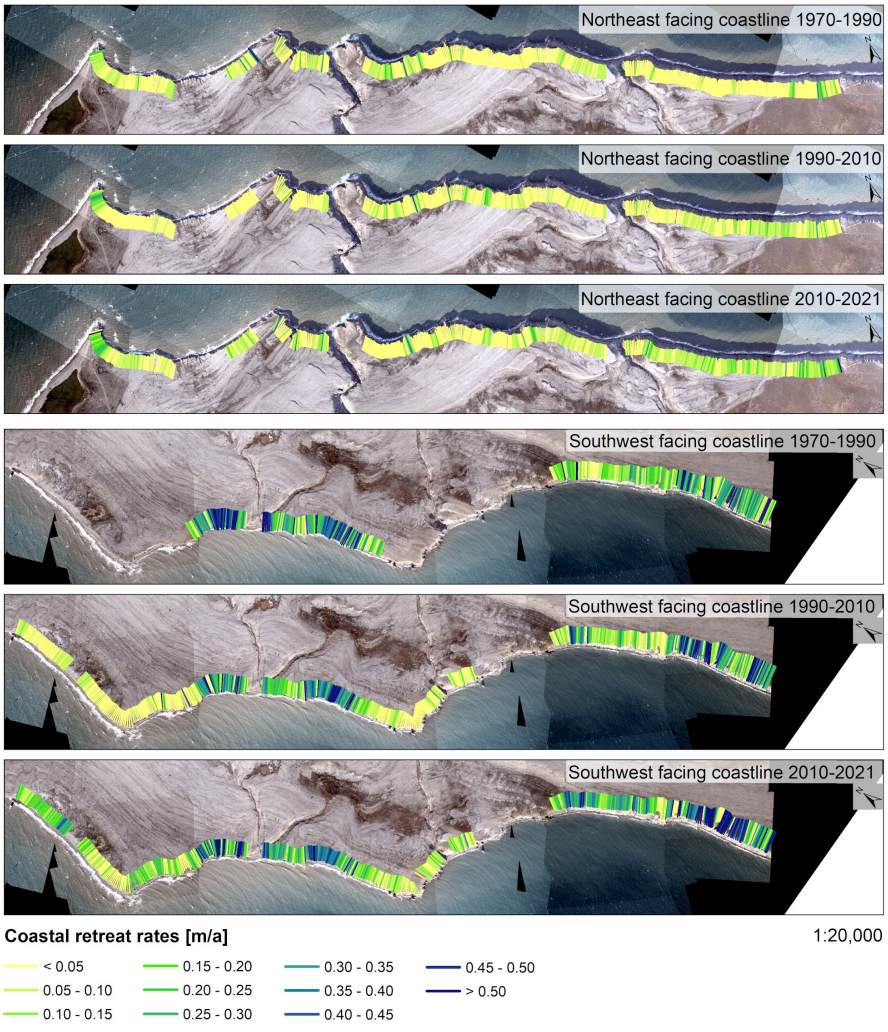

Figure 4. Coastal retreat rates at the northeast and southwest facing coastline of Brøgger peninsula for the time periods 1970-1990, 1990-2010 and 2010-2021. Source of the orthoimage: Svalbard Integrated Arctic Earth Observing Systems SIOS, however, not publicly available.

The northeast facing coastline can be considered fairly stable, but with an acceleration of erosion during the last decade. The time periods 1970-1990 and 1990-2010 show a coastal retreat rate in the same order of magnitude, with a mean retreat rate of $0.04 \pm 0.06\,\mathrm{m\ a^{-1}}$ and $0.04 \pm 0.04\,\mathrm{m\ a^{-1}}$, respectively. However, the number of transects recording erosion increases slightly from $47\,\%$ to $55\,\%$, indicating that only about half of the coastline is subject to erosion. Despite the low erosion on average, single transects can have up to $0.51\,\mathrm{m\ a^{-1}}$ (1970-1990) and $0.44\,\mathrm{m\ a^{-1}}$ (1990-2010), even though only $2\,\%$ (1970-1990) and $1\,\%$ (1990-2010) of the transects result in retreat rates of $0.20\,\mathrm{m\ a^{-1}}$ or more. The coastal retreat rate increases in the following

https://doi.org/10.5194/egusphere-2023-321
Preprint. Discussion started: 23 March 2023

Table 3. Mean retreat rates and associated statistics for the analyzed time periods. The analysis is performed separately for the northeast facing coastline, the southwest facing coastline and an extended part of the southwest facing coastline, where the coastline could not be detected in the image of 1970. T stands for transects, RR for retreat rate, DOA for dilution of accuracy, T_E for transects calculating erosion and P is the result of Student's *t*-test. We tested for the significance of acceleration (right tailed), only the *p*-value denoted with † is calculated for deceleration (left tailed).

Extent	Length [m]	No. of T	Time period	RR ± DOA [m a^{-1}]	T_E [%]	Max RR [m a^{-1}]	RR > 0.2 m a^{-1} [%]	*p*-value (*t*-test)
NE	2670	534	1970-1990	0.04 ± 0.06	47	0.51	2	0.409
			1990-2010	0.04 ± 0.04	55	0.44	1	2.5E-10
			2010-2021	0.06 ± 0.08	65	0.83	4	
SW	1730	346	1970-1990	0.26 ± 0.06	94	1.06	55	0.099†
			1990-2010	0.24 ± 0.04	92	1.28	52	1.4E-6
			2010-2021	0.30 ± 0.08	95	0.96	65	
SW ext.	2880	576	1970-1990	-	-	-	-	0.003
			1990-2010	0.16 ± 0.04	81	1.28	32	
			2010-2021	0.21 ± 0.08	89	0.96	45	

decade (2010-2021), indicating higher erosion, with a mean retreat rate of 0.06 ± 0.08 m a^{-1}. The acceleration in retreat rate between 1990-2010 and 2010-2021 is statistically significant ($p = 2.5 * 10^{-10}$). A retreat is calculated for 65 % of the transects, showing that a longer part of the coastline experiences erosion during that time span. This is visualized in Fig. 4: while yellow colors (retreat rates < 0.05 m a^{-1}, little to no erosion) dominate in 1970-1990, the number of bright green colored transects (retreat rates < 0.20 m a^{-1}) increases along the entire coastline in 2010-2021, indicating higher retreat rates. In addition, more transects show a retreat rate greater than 0.20 m a^{-1}, with a maximum of 0.83 m a^{-1}.

In contrast to retreat rates well below 0.10 m a^{-1} in the northeast facing sector, the southwest facing coastline is subject to more pronounced erosion. The highest retreat rates in the last decade are recorded here. While erosion decelerates slightly from 0.26 ± 0.06 m a^{-1} in 1970-1990 to 0.24 ± 0.04 m a^{-1} in 1990-2010, it accelerates statistically significantly ($p = 1.4 * 10^{-6}$) to 0.30 ± 0.08 m a^{-1} in the past decade (2010-2021). Almost the entire southwest facing coastline is subject to erosion during the analyzed time period (1970-2021) with over 90 % of the transects showing a retreat. In addition to the more intense erosion compared to the northeast facing coastline, the maximum retreat rate is also higher in all analyzed time periods with 1.06 m a^{-1} in 1970-1990, 1.28 m a^{-1} in 1990-2010 and 0.96 m a^{-1} in 2010-2021. Retreat rates of more than 0.20 m a^{-1} are obtained for 55 % (1970-1990), 52 % (1990-2010) and 65 % (2010-2021) of the transects. They are often concentrated in certain parts of the coastline and shift within the analyzed time periods. Therefore it is likely that not (only) a more susceptible bedrock or a specific exposition leads to a constantly increased erosion rate, but that large blocks are released in single events, increasing the mean retreat rate calculated in this study.

For the time periods 1990-2010 and 2010-2021 the retreat rate is estimated for a longer section (SW ext. in Table 3). Here the results show that the erosion accelerates significantly from 0.16 ± 0.04 m a^{-1} (1990-2010) to 0.21 ± 0.08 m a^{-1} (2010-2021).

https://doi.org/10.5194/egusphere-2023-321
Preprint. Discussion started: 23 March 2023

Furthermore, the percentage of transects that calculate retreat increase from 81 % to 89 %. These results indicate that lower retreat rates occur in this section, but they show the same trend of intensified erosion over the last decade 2010-2021.

4.3 Rock surface temperatures

The measurement period of the logger RW-SW close to Kjærsvika lasted from 1 September 2020 to 31 August 31 2021. During this period, the logger measured a mean annual rock surface temperatures of −0.49 °C. This indicates below-freezing temperatures, but average ground temperatures in the permafrost behind the rock wall are likely close to the freezing point. The mean seasonal values were −6.2 °C for winter (December to February), −3.1 °C for spring (March to May), 6.6 °C for summer (June to August) and 0.6 °C for fall (September to November). The lowest rock surface temperature at RW-SW was recorded on both 31 January and 16 March with a temperature of −14.7 °C, while the highest rock surface temperature was found on 3 August with 18.7 °C (Fig. 5). The daily variability in the rock surface temperature is more pronounced in the spring and summer seasons, showing high frequency variability and large amplitudes. In the fall and winter seasons, although the daily variability also has high amplitudes, the frequencies of the temperature fluctuations decrease.

The logger RW-SW is located at the southwest facing coastline of Brøgger peninsula, exposed to the open sea. Comparing its records to the logger RW04 (Schmidt et al., 2021) at the northeast facing coastline, which is protected from the open sea by Kongsfjorden, shows differences in mean annual rock surface temperatures. RW04 measures a value of −1.64 °C, which is 1.15 °C lower than RW-SW. The temperature differences are particularly pronounced in late winter and early spring. The entire measurement period is shown in Fig. 5.

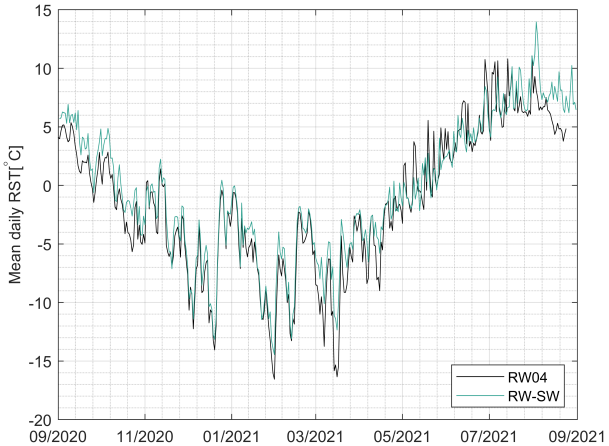

Figure 5. Measured rock surface temperature from September 1, 2020, to August 31, 2021 for both rock wall loggers at the northeast facing coast (RW04) and the southwest facing coast (RW-SW).

https://doi.org/10.5194/egusphere-2023-321
Preprint. Discussion started: 23 March 2023

5 Discussion

5.1 Comparison to previous studies

The mean coastal retreat rates indicate that the northeast facing coastline is fairly stable with mean annual values between $0.04 \pm 0.06\,\mathrm{m\,a^{-1}}$ and $0.06 \pm 0.08\,\mathrm{m\,a^{-1}}$ during the analyzed time period, while the southwest facing coastline is subject to more intense erosion with mean annual values between $0.24 \pm 0.04\,\mathrm{m\,a^{-1}}$ and $0.30 \pm 0.08\,\mathrm{m\,a^{-1}}$. Both cases show a statistically significant acceleration of erosion during the last decade 2010-2021. The calculated retreat rates are lower than the average change in Arctic coastlines of $0.5\,\mathrm{m\,a^{-1}}$ (Lantuit et al., 2013). However, the findings of this study suggest higher values than most previous studies on coastal cliff erosion in Svalbard. Prick (2004) reports retreat rates of $0.0019\,\mathrm{m\,a^{-1}}$ in coastal sandstone and shale cliffs in Longyearbyen using sediment traps and Wangensteen et al. (2007) detect a retreat of $0.0027\,\mathrm{m\,a^{-1}}$ and $0.0031\,\mathrm{m\,a^{-1}}$ with terrestrial photogrammetry in dolomitic limestone in Kongsfjorden area. Lim et al. (2020) find a higher retreat rate between $0.01\,\mathrm{m\,a^{-1}}$ and $0.019\,\mathrm{m\,a^{-1}}$ in marbles at Veslebogen, applying terrestrial laser scanning and photogrammetry. In contrast, the results of Guégan and Christiansen (2017) along bedrock overlain by unconsolidated sediments show retreat rates of $0.45\,\mathrm{m\,a^{-1}}$ to $0.80\,\mathrm{m\,a^{-1}}$ along a 100 m transect, which is larger than the mean but close to the maximum retreat rates found in this study. Differences in the retreat rates can be explained by various factors, such as (1) the applied method and considered time period, (2) lithology, and (3) fetch and wave activity as well as local climate conditions. However, the respective importance of each factor is difficult to determine.

(1) Most previous studies of coastal cliff erosion on Svalbard determined the retreat rate with either terrestrial photogrammetry or laserscanning. By doing so, volume erosion at the cliff face is detected by locating e.g. single rock falls. These methods are typically constrained in space in time due to narrow beaches and a lack of historical data, so that the results are highly dependent on the selected location and year of measurement. In contrast to that, we only consider the retreat rate at the top of the cliff, but extent the analysis over a much longer segment of the coastline ($5.5\,\mathrm{km}$) and a longer time period (1970-2021). By choosing a close spacing of $5\,\mathrm{m}$ of the transects, we ensure to capture small irregularities along the coastline. Consequently, we measure a different parameter and over different scales in time and space compared to previous studies, which may result in different retreat rates.

(2) Varying bedrock characteristics can lead to large differences in coastal retreat rates. Global averages for erosion rates for limestone are typically within the range of $0.001 - 0.01\,\mathrm{m\,a^{-1}}$ and for shale around $0.01\,\mathrm{m\,a^{-1}}$ (Sunamura, 1992). The results of this study show much higher retreat rates, which could be explained by the coastal environment and associated abrasion together with the removal of the eroded material at the base of the cliff. While the spatially constrained methods of previous studies on Svalbard can describe the bedrock type in more detail and are often limited to one rock type, the coastal cliffs in this study consist of conglomerates, sandstones, shales, and carbonates. A detailed characterization of the lithology along the coastline of Brøgger peninsula would enable better comparison with previous studies. However, such a mapping is beyond the scope of this study.

(3) The local setting plays an important role in coastal cliff erosion. The wave activity may differ markedly between field sites, depending on the exposure to the open ocean and the fetch, as well as duration of sea ice cover and the development of an

https://doi.org/10.5194/egusphere-2023-321
Preprint. Discussion started: 23 March 2023

ice-foot (Irrgang et al., 2022; Wangensteen et al., 2007). Furthermore, variations in climate variables such as air temperatures and radiation can influence the thermal regime of the bedrock and therefore its susceptibility towards erosion (Krautblatter et al., 2013). As all these factors can vary on a small scale across Svalbard (Hanssen-Bauer et al., 2019), previous studies are well expected to result in different retreat rates.

5.2 Coastal retreat rates under a warming climate

Retreat rates of Arctic coastlines are governed by various drivers, dependent on the local coastal setting and environmental conditions (Irrgang et al., 2022). The lower part of the coastal cliffs are prone to abrasion, acting through the thermal and wave-driven mechanical energy of the sea (Are, 1988b, a) and intensive wetting-drying during open-water season (Strzelecki et al., 2017). We assume that these factors play an important role in coastal erosion along Brøgger peninsula, as overhanging rock walls with a retreated foot of the cliff can be observed (Fig. 1c). Abrasion is especially effective during stormy weather, which intensified in the area around Brøgger peninsula during the past decades. The number of recorded days with a wind speed of more than $10.8\,\mathrm{m\,s^{-1}}$ (i.e., at least a strong breeze) increased in Ny-Ålesund by about five days per decade (see appendix), of which most occurred during winter. Furthermore, extreme cyclone events regularly occur in the Arctic North Atlantic, with 20 to 40 events during winter. In Ny-Ålesund, an increasing trend of six cyclones per decade was detected from 1979-2015, which can be related to a decreasing sea ice extent in the region and large-scale atmospheric circulation changes (Rinke et al., 2017). Single weather events like this can support the release of large blocks and consequently, they can have a localized but pronounced influence on the retreat rates.

The effect of abrasion is dependent on the length of open water season. Dahlke et al. (2020) provides an overview of sea ice extent across Svalbard from 1980 to 2016. The results show a considerable decrease in sea ice coverage during winter and spring in Forlandsundet (southwest facing coastline), falling from $50-70\,\%$ until the early 2000s to below $10\,\%$ in recent years. Kongsfjorden (northeast facing coastline) experienced an increase in sea ice extent from around $40\,\%$ to $60\,\%$ in the 1990s and a subsequent decrease to around $10\,\%$. However, as the analyzed field area in this study is located in the outer parts of Kongsfjorden (NE sector) and near the open Arctic ocean (SW sector), where typically less sea ice develops, so that even lower percentages of sea ice coverage are likely. The lengthening of the open water season allows for an increased wind-driven wave action, intensifying the abrasion at the coastal cliffs of Brøgger peninsula, and hence, resulting potentially in larger retreat rates in recent years. As the southwest facing coastline is exposed to the open sea, while the northeast facing coastline is protected by Kongsfjorden, differences in coastal retreat rates could be largely explained by a longer fetch and enhanced wave action along the former.

Under ongoing atmospheric warming in the last decades, increasing ground temperatures have been measured on Svalbard (Boike et al., 2018; Christiansen et al., 2010; Etzelmüller et al., 2020; Isaksen et al., 2007). Furthermore, retreating sea ice coverage and a consequently ice-free water body can warm coastal rock walls through additional longwave energy input (Schmidt et al., 2021). Higher ground temperatures can affect the stability of permafrost rock walls (Krautblatter et al., 2013). Rock surface measurements in 2020/2021 along the coastline of Brøgger peninsula show that the permafrost is close to the thaw threshold, with especially high values at the southwest facing coastline, falling into a temperature range with decreased

https://doi.org/10.5194/egusphere-2023-321
Preprint. Discussion started: 23 March 2023

stability (Davies et al., 2001). Due to limited snow accumulation in the steep coastal cliffs, the rock surface temperature is mainly linked to air temperature as well as longwave and shortwave radiation. Topographically downscaled ERA5 climate data (Fiddes and Gruber, 2014; Hersbach et al., 2020; Renette et al., 2023) for Brøgger peninsula show that air temperature and longwave radiation increased over the past decades, while shortwave radiation decreases slightly (see appendix). The latter is much stronger at the southwest facing coastline (see appendix), contributing to higher rock surface temperatures at logger RW-SW. If this trend continues, we expect a further increase in rock temperatures in the coastal cliffs of Brøgger peninsula, potentially making the rock more susceptible to erosion.

The coastal cliffs stabilize the unconsolidated material on top. Analysis of the orthoimages show that the top of the cliff retreats typically in conjunction with the bedrock and consequently, the erosion of the sediments is highly dependent on the retreat of the bedrock below. Nevertheless, more annual rainfall (see appendix) can result in increased overland flow, forming channels on the surface and erosional gullies (Jorgenson and Osterkamp, 2005), which enhance the mechanical erosion of the sediments. The development of these features can occur either rapidly or evolve over longer time periods (Fortier et al., 2007; Godin and Fortier, 2012). Observations along the coastline in the field show locally the occurrence of such channels and the analysis of the orthoimages show, that the gullies develop over several decades.

Although the data in this study do not allow to relate the retreat rates directly to records of weather stations or downscaled climate data, we can observe that the acceleration of the retreat rate coincides with increasing storminess and retreating sea ice, which may enhance coastal erosion, together with increasing ground temperatures, which may lead to an increased susceptibility of the coastline.

6 Conclusions

In this study, we calculate retreat rates of the coastal rock cliffs along Brøgger peninsula, Svalbard, based on aerial orthoimages from the years 1970, 1990, 2010 and 2021. While previous studies on coastal erosion on Svalbard are spatially and temporally limited, we present long-term trends in coastal retreat rates, covering several kilometers along Brøgger peninsula. The main conclusions are as follows:

- At the northeast facing coastline, we detect fairly stable conditions, however with an increasing trend in the retreat rate from $0.04 \pm 0.06\,\mathrm{m\ a^{-1}}$ (1970-1990) and $0.04 \pm 0.04\,\mathrm{m\ a^{-1}}$ (1990-2010) to $0.06 \pm 0.08\,\mathrm{m\ a^{-1}}$ (2010-2021). About half of the transects show erosion, increasing from $47\,\%$ (1970-1990) over $55\,\%$ (1990-2010) to $65\,\%$ (2010-2021).

- In contrast, the southwest facing coastline shows higher retreat rates with $0.26 \pm 0.06\,\mathrm{m\ a^{-1}}$ from 1970 to 1990, a decrease to $0.24 \pm 0.04\,\mathrm{m\ a^{-1}}$ in 1990-2010 and an statistically significant acceleration in retreat rates to $0.30 \pm 0.08\,\mathrm{m\ a^{-1}}$ in the past decade from 2010 to 2021. More than $90\,\%$ of the southwest facing coastline is affected by erosion during the entire time period.

- Installed temperature loggers recorded rock surface temperatures in the time period September 2020 to September 2021. Permafrost conditions are close to the thaw threshold with a mean annual rock surface temperature of $-0.49\,°\mathrm{C}$ at the

https://doi.org/10.5194/egusphere-2023-321
Preprint. Discussion started: 23 March 2023

southwest facing coastline, while mean annual rock surface temperature along the northeast facing coastline in Ny-Ålesund are lower with $-1.64\,°C$.

- The coastal cliffs of Brøgger peninsula are exposed to changing climatic conditions, in particular, increasing storminess and retreating sea ice, but also warming permafrost and increasing rainfall. These factors can explain the accelerating coastal erosion measured over the past decade.

https://doi.org/10.5194/egusphere-2023-321
Preprint. Discussion started: 23 March 2023

Appendix A: Topography-based downscaling of atmospheric reanalysis data and climate change detection

To investigate links between the coastal erosion dynamics at the Brøgger peninsula and possible changes in the local climate, we use hourly ERA5 reanalysis data (Hersbach et al., 2020) in conjunction with a downscaling routine. The ERA5 reanalysis data can relatively accurately represent the mesoscale (scales 10-100 km) behavior of the atmosphere and the underlying surface. To take into account hillslope scale effects we used the topography-based downscaling routine TopoSCALE (Fiddes and Gruber, 2014). This scheme has been widely used for downscaling reanalysis data in complex terrain (e.g. Renette et al., 2023). TopoSCALE uses several terrain parameters (elevation, slope, aspect, sky view factor, and horizon angles) to adjust coarse scale meteorological forcing to a finer grid that can represent local topography.

The terrain parameters were computed using a 30 m resolution DEM of Svalbard (Norwegian Polar Institute, 2014a), focusing on 6 sites: the Ny-Ålesund weather station (SN99910), the Ny-Ålesund BSRN station, the Bayelva climate station (BCS), Stuphallet, Kongsfjordneset, and Kjærsvika. While the three latter sites represent coastal cliffs, the first three were used for validation as shown in Fig. A1. The downscaling performed well at a monthly time-scale for air temperature (validated against SN99910), specific humidity with a slight tendency to underestimate periods with higher humidity (validated against BCS), incoming shortwave and longwave radiation (validated against BCS) and provided a very accurate estimate of surface pressure (validated against BSRN). Although we did not perform a direct validation of the downscaled precipitation, due to challenges in measuring this variable, the performance for surface pressure suggests that ERA5 is able to capture larger scale synoptic precipitation events. The evaluation of wind speed showed a larger scatter, so that station data was used to when looking into trends in storminess (Fig. B1), provided by the Norwegian Meteorological Institute (https://seklima.met.no/).

We aggregated the hourly downscaled data to represent annual means (temperature, incoming longwave, incoming shortwave) and accumulations (snowfall and rainfall). Annual snowfall and rainfall were estimated using an air temperature-based phase delineation of hourly precipitation. The annual aggregation leads to a further reduction in RMSE compared to the monthly estimates given in Fig. A1. The annual error is thus likely low enough for detecting multi-decadal climate change signals. For all variables but incoming shortwave radiation and days with storminess we take the average across the three study sites (Stuphallet, Kjærsvika, and Kongsfjordneset) for the downscaled ERA5 data from 1950 to 2021. For incoming shortwave radiation we use the same data and period but consider two sites with different exposition (Stuphallet: north east facing, Kjærsvika: south west facing) separately. For days with storminess, we use data from the Ny-Ålesund meteorological station.

To detect trends in the annual time series, we performed a Bayesian regression analysis (Särkkä, 2013) which is an established method for climate change detection (Annan, 2010). In particular, we fit two competing models: a "trend" model with a linearly varying background climate and a "steady" model with a fixed background climate.

The regression analysis of the trend model delivers the trend coefficients β and the scales of internal climate variability σ. As a verification, we expect around 5% of the data to fall outside the red 95% predictive interval, which is what we see for all panels in Fig. B1. For each variable we also report the Bayes factor (Kass and Raftery, 1995), denoted B, which quantifies how much support the data lend to the trend model versus the steady model. This is output on a logarithmic scale measuring the weight of evidence in favor of a trend: $0 < \log_{10}(B) < 0.5$ is *weak* evidence, $0.5 < \log_{10}(B) < 1$ is *substantial* evidence,

https://doi.org/10.5194/egusphere-2023-321
Preprint. Discussion started: 23 March 2023

$1 < \log_{10}(B) < 2$ is *strong* evidence, and $\log_{10}(B) > 2$ is *decisive* evidence. For negative $\log_{10}(B)$ the scale is the same but in favor of no trend (the steady model). For our analysis, $\log_{10}(B)$ can thus help quantify the strength of evidence in favor of (or against if $\log_{10}(B) < 0$) a climate change signal over the last 70 years.

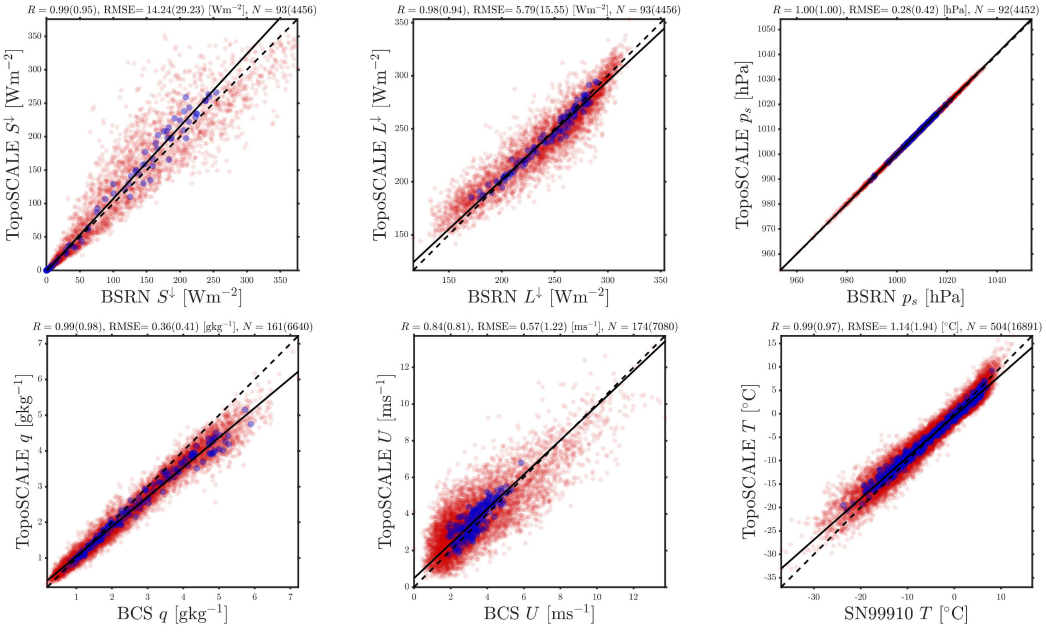

Figure A1. Validation of the downscaled data at stations (BSRN, BCS, SN99910) near Ny-Ålesund: Incoming shortwave (top left), incoming longwave (top middle), surface pressure (top right), specific humidity (bottom left), wind speed (bottom middle), and air temperature (bottom right). Red dots: daily averages; blue dots: monthly averages; dashed line: identity; solid line: linear best fit. Stations with the longest records were selected in each case. The correlation coefficient (R), RMSE, and number of points at the monthly (daily) scale are in the panel titles.

Appendix B: Trends in climatic parameters for the Brøgger Peninsula

The outputs from the regression analysis for the trend model are shown in Fig. B1. The air temperature shows a decisive positive trend with +0.6 °C per decade, increasing from approximately -7 °C to -3 °C. A strong increase in annual rainfall is detected with 13 mm per decade. The values increase from about 180 mm in the 1950s to 270 mm in the last decade. As this analysis only considers annual values, no conclusion can be drawn regarding the occurrence of heavy rainfall events. In contrast to that, there is substantial evidence that the amount of snowfall is staying steady with only a very slight decrease of -2.7 mm per decade with a nearly constant climatology around 280 mm per year. The strongly increasing trend in rainfall and negligible decreasing trend in snowfall indicate an overall warmer and wetter climate.

The incoming longwave radiation shows a decisive increasing trend in the last 70 years with 1.6 W/m^2 per decade. The mean annual values increase on average from 227 W/m^2 in the 1950s to 237 W/m^2 in recent years. The increase in longwave radiation

https://doi.org/10.5194/egusphere-2023-321
Preprint. Discussion started: 23 March 2023

has a pronounced effect on the surface energy balance, with more energy being transferred to the ground surface. The steep slope angles of the coastal cliffs influence the incoming shortwave radiation. Mean annual values at Kjærsvika (representative field site for the southwest facing coastline) decrease strongly from 83 W/m^2 to 78 W/m^2 with -0.8 W/m^2 per decade. With a substantial trend of -0.6 W/m^2 per decade, Stuphallet shows a trend in the same order of magnitude, however, the incoming shortwave radiation is considerably lower, decreasing from 70 W/m^2 to 67 W/m^2. The reduced incoming shortwave radiation at Stuphallet is a result of the northeast exposition of the coastline resulting in longer periods of shading.

Due to challenges with downscaling wind data, the increase in storminess is analyzed with station data in Ny-Ålesund, Svalbard, located in approximately seven kilometers of the field site. Days with wind speeds larger than 10.8 m/s (strong breeze or stronger) increased by 5.3 days per decade since 1974. Years with exceptionally many days with high wind speeds occurred in the early 1990s, while they decreased slightly in recent years. The evidence in favor of this increase is weak, however, and not worth more than a bare mention on the Bayes factor scale.

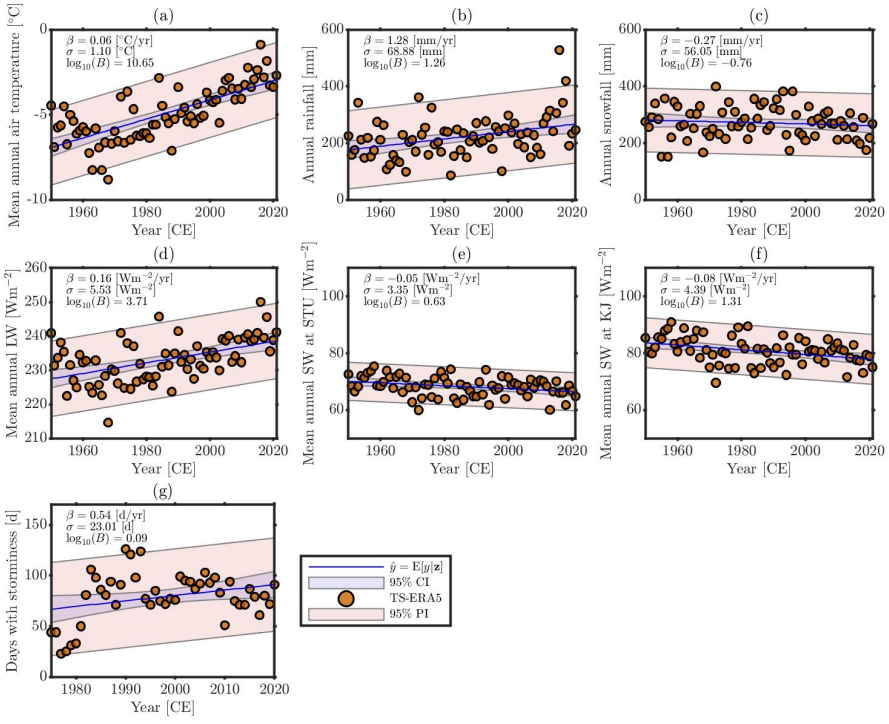

Figure B1. Climate on the Brøgger Peninsula for the last decades from downscaled from ERA5 data (a-f) and Ny-Ålesund station data (g): (a) Air temperature, (b) Rainfall, (c) Snowfall, (d) Incoming longwave radiation, (e) Incoming shortwave radiation at Stuphallet and (f) at Kjærsvika, (g) days with wind speeds larger than 10.8 ms^{-1}. Annual data: orange dots; mean background climate: blue line; 95% credible interval for the background climate: blue shading; 95% predictive interval including internal variability: red shading.

https://doi.org/10.5194/egusphere-2023-321
Preprint. Discussion started: 23 March 2023

Data availability. The dGNSS survey and the analysis of the multiple digitization of the coastline are archived on zenodo (https://doi.org/10.5281/zenodo.7756973, Aga, 2023). The orthoimage of 2010 can be accessed at https://geodata.npolar.no/, whereas the orthoimages of 1970, 1990 and 2021 are not publicly available.

Author contributions. JA designed the concept of the study, conducted field work, performed the DSAS analysis and prepared the manuscript with all tables and figures. LP contributed to the concept during all phases of the study and digitized the coastlines. SW provided ideas regarding the concept of the study as well as organizational and technical support. LP and AK acquired the aerial images. LG processed the aerial images. TE performed the post-processing of the dGNSS data. JA and KA performed the statistical tests. KA downscaled the climate data and prepared most of the appendix. All authors contributed to the final manuscript with input and suggestions.

Competing interests. There are no competing interests.

Acknowledgements. We acknowledge funding by EU Horizon 2020 ("Nunataryuk", grant no. 773421), the Research Council of Norway (Arctic Field Grant "Coastal erosion on the Brøgger peninsula, Svalbard", grant no. 321957 and "PCCH-Arctic", grant no. 320769). Furthermore, we acknowledge the support of Robin B. Zweigel during fieldwork.

https://doi.org/10.5194/egusphere-2023-321
Preprint. Discussion started: 23 March 2023

References

Ambaum, M. H.: Significance tests in climate science, Journal of Climate, 23, 5927–5932, https://doi.org/10.1175/2010JCLI3746.1, 2010.

Annan, J.: Bayesian approaches to detection and attribution, WIREs Climate Change, https://doi.org/10.1002/wcc.47, 2010.

Are, F.: Thermal abrasion of sea coasts (Part II), https://doi.org/10.1080/10889378809377352, 1988a.

Are, F. E.: Thermal abrasion of sea coasts (part I), https://doi.org/10.1080/10889378809377343, 1988b.

Benjamin, D. J., Berger, J. O., Johannesson, M., Nosek, B. A., Wagenmakers, E.-J., Berk, R., Bollen, K. A., Brembs, B., Brown, L., Camerer, C., et al.: Redefine statistical significance, Nature human behaviour, 2, 6–10, https://doi.org/10.1038/s41562-017-0189-z, 2018.

Biskaborn, B. K., Smith, S. L., Noetzli, J., Matthes, H., Vieira, G., Streletskiy, D. A., Schoeneich, P., Romanovsky, V. E., Lewkowicz, A. G., Abramov, A., et al.: Permafrost is warming at a global scale, Nature communications, 10, 1–11, https://doi.org/10.1038/s41467-018-08240-4, 2019.

Boike, J., Juszak, I., Lange, S., Chadburn, S., Burke, E., Overduin, P. P., Roth, K., Ippisch, O., Bornemann, N., Stern, L., et al.: A 20-year record (1998–2017) of permafrost, active layer and meteorological conditions at a high Arctic permafrost research site (Bayelva, Spitsbergen), Earth System Science Data, 10, 355–390, https://doi.org/10.5194/essd-10-355-2018, 2018.

Christiansen, H. H., Etzelmüller, B., Isaksen, K., Juliussen, H., Farbrot, H., Humlum, O., Johansson, M., Ingeman-Nielsen, T., Kristensen, L., Hjort, J., et al.: The thermal state of permafrost in the nordic area during the international polar year 2007–2009, Permafrost and Periglacial Processes, 21, 156–181, https://doi.org/https://doi.org/10.1002/ppp.687, 2010.

Dahlke, S., Hughes, N. E., Wagner, P. M., Gerland, S., Wawrzyniak, T., Ivanov, B., and Maturilli, M.: The observed recent surface air temperature development across Svalbard and concurring footprints in local sea ice cover, International Journal of Climatology, 40, 5246–5265, https://doi.org/10.1002/joc.6517, 2020.

Davies, M. C., Hamza, O., and Harris, C.: The effect of rise in mean annual temperature on the stability of rock slopes containing ice-filled discontinuities, Permafrost and periglacial processes, 12, 137–144, https://doi.org/10.1002/ppp.378, 2001.

Etzelmüller, B., Ødegård, R., and Sollid, J.: The spatial distribution of coast types on Svalbard, in: Arctic Coastal Dynamics–Report of the 3rd International Workshop. Extended Abstracts. Alfred Wegener Institute for Po- lar and Marine Research, Bremerhaven, pp. 33–40, Citeseer, 2003.

Etzelmüller, B., Guglielmin, M., Hauck, C., Hilbich, C., Hoelzle, M., Isaksen, K., Noetzli, J., Oliva, M., and Ramos, M.: Twenty years of European mountain permafrost dynamics—the PACE legacy, Environmental Research Letters, 15, 104 070, https://doi.org/10.1088/1748-9326/abae9d, 2020.

Fiddes, J. and Gruber, S.: TopoSCALE v.1.0: downscaling gridded climate data in complex terrain, Geoscientific Model Development, 7, 387–405, https://doi.org/10.5194/gmd-7-387-2014, 2014.

Fortier, D., Allard, M., and Shur, Y.: Observation of rapid drainage system development by thermal erosion of ice wedges on Bylot Island, Canadian Arctic Archipelago, Permafrost and Periglacial Processes, 18, 229–243, https://doi.org/10.1002/ppp.595, 2007.

Fritz, M., Vonk, J. E., and Lantuit, H.: Collapsing arctic coastlines, Nature Climate Change, 7, 6–7, https://doi.org/10.1038/nclimate3188, 2017.

Gerland, S. and Hall, R.: Variability of fast-ice thickness in Spitsbergen fjords, Annals of Glaciology, 44, 231–239, https://doi.org/10.3189/172756406781811367, 2006.

Girod, L. and Filhol, S.: luc-girod/MicMacWorkflowsByLucGirod: As of processing of Sedongpu glacier in (Kääb and Girod, 2022 or 2023), https://doi.org/10.5281/zenodo.7380304, 2022.

https://doi.org/10.5194/egusphere-2023-321
Preprint. Discussion started: 23 March 2023

Godin, E. and Fortier, D.: Geomorphology of a thermo-erosion gully, Bylot Island, Nunavut, Canada, Canadian Journal of Earth Sciences, 49, 979–986, https://doi.org/10.1139/e2012-015, 2012.

Guégan, E. B. and Christiansen, H. H.: Seasonal Arctic coastal bluff dynamics in Adventfjorden, Svalbard, Permafrost and Periglacial Processes, 28, 18–31, https://doi.org/10.1002/ppp.1891, 2017.

Günther, F., Overduin, P. P., Sandakov, A. V., Grosse, G., and Grigoriev, M. N.: Short-and long-term thermo-erosion of ice-rich permafrost coasts in the Laptev Sea region, Biogeosciences, 10, 4297–4318, https://doi.org/10.5194/bg-10-4297-2013, 2013.

Hanssen-Bauer, I., Førland, E., Hisdal, H., Mayer, S., Sandø, A., Sorteberg, A., Adakudlu, M., Andresen, J., Bakke, J., Beldring, S., Benestad, R., van der Bilt, W., Bogen, J., Borstad, C., Breili, K., Breivik, O., Børsheim, K., Christiansen, H., Dobler, A., and Wong, W.: Climate in Svalbard 2100 - A knowledge base for climate adaptation, NCCS report, https://doi.org/10.13140/RG.2.2.10183.75687, 2019.

Hersbach, H. et al.: The ERA5 global reanalysis, Quarterly Journal of the Royal Meteorological Society, 146, 1999–2049, https://doi.org/https://doi.org/10.1002/qj.3803, 2020.

Himmelstoss, E. A., Henderson, R. E., Kratzmann, M. G., and Farris, A. S.: Digital shoreline analysis system (DSAS) version 5.1 user guide, Tech. rep., US Geological Survey, https://doi.org/10.3133/ofr20211091, 2021.

Hop, H. and Wiencke, C.: The Ecosystem of Kongsfjorden, Svalbard, in: The Ecosystem of Kongsfjorden, Svalbard, pp. 1–20, Springer, https://doi.org/10.1007/978-3-319-46425-1_1, 2019.

Irrgang, A. M., Lantuit, H., Manson, G. K., Günther, F., Grosse, G., and Overduin, P. P.: Variability in rates of coastal change along the Yukon coast, 1951 to 2015, Journal of Geophysical Research: Earth Surface, 123, 779–800, https://doi.org/10.1002/2017JF004326, 2018.

Irrgang, A. M., Bendixen, M., Farquharson, L. M., Baranskaya, A. V., Erikson, L. H., Gibbs, A. E., Ogorodov, S. A., Overduin, P. P., Lantuit, H., Grigoriev, M. N., et al.: Drivers, dynamics and impacts of changing Arctic coasts, Nature Reviews Earth & Environment, 3, 39–54, https://doi.org/10.1038/s43017-021-00232-1, 2022.

Isaksen, K., Sollid, J. L., Holmlund, P., and Harris, C.: Recent warming of mountain permafrost in Svalbard and Scandinavia, Journal of Geophysical Research: Earth Surface, 112, https://doi.org/10.1029/2006JF000522, 2007.

Isaksen, K., Nordli, Ø., Førland, E. J., Łupikasza, E., Eastwood, S., and Niedźwiedź, T.: Recent warming on Spitsbergen—Influence of atmospheric circulation and sea ice cover, Journal of Geophysical Research: Atmospheres, 121, 11–913, https://doi.org/10.1002/2016JD025606, 2016.

Johansson, A. M., Malnes, E., Gerland, S., Cristea, A., Doulgeris, A. P., Divine, D. V., Pavlova, O., and Lauknes, T. R.: Consistent ice and open water classification combining historical synthetic aperture radar satellite images from ERS-1/2, Envisat ASAR, RADARSAT-2 and Sentinel-1A/B, Annals of Glaciology, 61, 40–50, https://doi.org/10.1017/aog.2019.52, 2020.

Jones, B. M., Farquharson, L. M., Baughman, C. A., Buzard, R. M., Arp, C. D., Grosse, G., Bull, D. L., Günther, F., Nitze, I., Urban, F., et al.: A decade of remotely sensed observations highlight complex processes linked to coastal permafrost bluff erosion in the Arctic, Environmental Research Letters, 13, 115 001, https://doi.org/10.1088/1748-9326/aae471, 2018.

Jorgenson, M. and Osterkamp, T.: Response of boreal ecosystems to varying modes of permafrost degradation, Canadian Journal of Forest Research, 35, 2100–2111, https://doi.org/10.1139/x05-153, 2005.

Kass, R. and Raftery, A.: Bayes Factors, J. Am. Stat. Assoc., https://doi.org/10.2307/2291091, 1995.

Krautblatter, M., Funk, D., and Günzel, F. K.: Why permafrost rocks become unstable: a rock–ice-mechanical model in time and space, Earth Surface Processes and Landforms, 38, 876–887, https://doi.org/10.1002/esp.3374, 2013.

Lantuit, H., Overduin, P., and Wetterich, S.: Recent progress regarding permafrost coasts, Permafrost and periglacial processes, 24, 120–130, https://doi.org/10.1002/ppp.1777, 2013.

https://doi.org/10.5194/egusphere-2023-321
Preprint. Discussion started: 23 March 2023

Lim, M., Strzelecki, M. C., Kasprzak, M., Swirad, Z. M., Webster, C., Woodward, J., and Gjelten, H.: Arctic rock coast responses under a changing climate, Remote sensing of environment, 236, 111 500, https://doi.org/10.1016/j.rse.2019.111500, 2020.

Maturilli, M., Herber, A., and König-Langlo, G.: Surface radiation climatology for Ny-Ålesund, Svalbard (78.9 N), basic observations for trend detection, Theoretical and Applied Climatology, 120, 331–339, https://doi.org/10.1007/s00704-014-1173-4, 2015.

Nordli, Ø., Wyszyński, P., Gjelten, H., Isaksen, K., Łupikasza, E., Niedźwiedź, T., and Przybylak, R.: Revisiting the extended Svalbard Airport monthly temperature series, and the compiled corresponding daily series 1898–2018, Polar Research, 39, https://doi.org/10.33265/polar.v39.3614, 2020.

Norwegian Meteorological Institute: Annual precipitation in Svalbard, Hopen and Jan Mayen, filtered. Environmental monitoring of Svalbard and Jan Mayen (MOSJ), http://www.mosj.no/en/climate/atmosphere/temperature-precipitation.html, last access: 04.07.2022, 2022.

Norwegian Polar Institute: Terrengmodell Svalbard (S0 Terrengmodell), https://doi.org/10.21334/npolar.2014.dce53a47, 2014a.

Norwegian Polar Institute: Terrengmodell Svalbard (S0 Terrengmodell), https://doi.org/10.21334/npolar.2014.dce53a47, 2014b.

Overeem, I., Anderson, R. S., Wobus, C. W., Clow, G. D., Urban, F. E., and Matell, N.: Sea ice loss enhances wave action at the Arctic coast, Geophysical Research Letters, 38, https://doi.org/10.1029/2011GL048681, 2011.

Prick, A.: Observations of rock temperatures and rock moisture variability in Longyearbyen: implications for cryogenic weathering and rock wall retreat rate, Abstracts of Pace 21: Permafrost and Climate in the 21st Century. Field Workshop Longyearbyen, Svalbard, 8-13 September 2004. P. 16. Longyearbyen: University Courses on Svalbard, 2004.

Radosavljevic, B., Lantuit, H., Pollard, W., Overduin, P., Couture, N., Sachs, T., Helm, V., and Fritz, M.: Erosion and flooding—threats to coastal infrastructure in the Arctic: a case study from Herschel Island, Yukon Territory, Canada, Estuaries and Coasts, 39, 900–915, https://doi.org/10.1007/s12237-015-0046-0, 2016.

Renette, C., Aalstad, K., Aga, J., Zweigel, R. B., Etzelmüller, B., Lilleøren, K. S., Isaksen, K., and Westermann, S.: Simulating the effect of subsurface drainage on the thermal regime and ground ice in blocky terrain in Norway, Earth Surface Dynamics, 11, 33–50, https://doi.org/10.5194/esurf-11-33-2023, 2023.

Rinke, A., Maturilli, M., Graham, R. M., Matthes, H., Handorf, D., Cohen, L., Hudson, S. R., and Moore, J. C.: Extreme cyclone events in the Arctic: Wintertime variability and trends, Environmental Research Letters, 12, 094 006, https://doi.org/10.1088/1748-9326/aa7def, 2017.

Rupnik, E., Daakir, M., and Pierrot Deseilligny, M.: MicMac - a free, open-source solution for photogrammetry, Open Geospatial Data, Software and Standards, 2, 1–9, 2017.

Särkkä, S.: Bayesian Filtering and Smoothing, Cambridge University Press, https://doi.org/10.1017/CBO9781139344203, 2013.

Schmidt, J. U., Etzelmüller, B., Schuler, T. V., Magnin, F., Boike, J., Langer, M., and Westermann, S.: Surface temperatures and their influence on the permafrost thermal regime in high-Arctic rock walls on Svalbard, The Cryosphere, 15, 2491–2509, https://doi.org/10.5194/tc-15-2491-2021, 2021.

Strzelecki, M., Kasprzak, M., Lim, M., Swirad, Z., Jaskólski, M., Modzel, P., et al.: Cryo-conditioned rocky coast systems: A case study from Wilczekodden, Svalbard, Science of The Total Environment, 607, 443–453, https://doi.org/10.1016/j.scitotenv.2017.07.009, 2017.

Student: The probable error of a mean, Biometrika, pp. 1–25, https://doi.org/10.2307/2331554, 1908.

Sunamura, T.: Geomorphology of rocky coasts, vol. 3, Wiley, 1992.

Takasu, T. and Yasuda, A.: Development of the low-cost RTK-GPS receiver with an open source program package RTKLIB, in: International symposium on GPS/GNSS, vol. 1, International Convention Center Jeju Korea, 2009.

https://doi.org/10.5194/egusphere-2023-321
Preprint. Discussion started: 23 March 2023

Tanski, G., Lantuit, H., Ruttor, S., Knoblauch, C., Radosavljevic, B., Strauss, J., Wolter, J., Irrgang, A. M., Ramage, J., and Fritz, M.: Transformation of terrestrial organic matter along thermokarst-affected permafrost coasts in the Arctic, Science of the Total Environment, 581, 434–447, https://doi.org/10.1016/j.scitotenv.2016.12.152, 2017.

Walczowski, W. and Piechura, J.: Influence of the West Spitsbergen Current on the local climate, International journal of climatology, 31, 1088–1093, https://doi.org/10.1002/joc.2338, 2011.

Wangensteen, B., Eiken, T., Ødegård, R. S., and Ludvig Sollid, J.: Measuring coastal cliff retreat in the Kongsfjorden area, Svalbard, using terrestrial photogrammetry, Polar Research, 26, 14–21, https://doi.org/10.1111/j.1751-8369.2007.00002.x, 2007.